

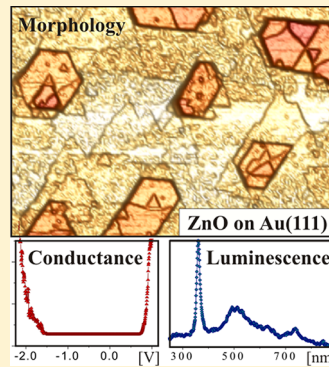
Morphology and Luminescence of ZnO Films Grown on a Au(111) Support

Fernando Stavale,[†] Leandro Pascua,[†] Niklas Nilius,^{*,†,‡} and Hans-Joachim Freund[†]

[†]Fritz-Haber-Institut der Max-Planck-Gesellschaft, Faradayweg 4-6, D-14195 Berlin, Germany

[‡]Carl von Ossietzky Universität Oldenburg, Institut für Physik, D-26111 Oldenburg, Germany

ABSTRACT: Using scanning tunneling microscopy and spectroscopy, we have analyzed the growth of ZnO thin films on a Au(111) support. Because of the 12% lattice mismatch with the metal beneath, ZnO develops a (0001)-oriented coincidence lattice that gives rise to a well-ordered hexagonal Moiré pattern with 2.2 nm periodicity. This superstructure disappears at 4 ML film thickness, when wide, atomically flat terraces delimited by straight monatomic steps become detectable in the STM. The long-range order of the films is deduced from sharp hexagonal spot patterns in low-energy electron diffraction. STM-based luminescence and conductance spectroscopy reveals that the ZnO band gap approaches the bulk value in films thicker than 10 ML. Additional photon peaks with sub-band-gap energies indicate the presence of defects in the wurzite lattice. The intrinsic polarity of the ZnO(0001) surface is accounted for by a reduced Zn–O interlayer distance and an adsorption-mediated compensation scheme in thin and thick films, respectively.



1. INTRODUCTION

ZnO is a promising material for the fabrication of high-speed electro-optical devices.¹ Its band gap of 3.37 eV is of a direct nature and thus ideally suited to interact with visible light. The gap size has shown to be tunable via doping the wurzite lattice with various cations and anions, such as Mg,^{2,3} Cr,⁴ and N.⁵ The donor and acceptor levels produced in this way open up new electron recombination channels and give rise to additional optical transitions with photon energies inside the fundamental band gap. ZnO also features higher electron mobility with respect to other oxides and is, therefore, particularly interesting for the fabrication of electronic devices. To use this potential, large efforts were undertaken to build structures with n- and p-type conductance behavior. Whereas n-type ZnO forms due to spontaneous hydrogen incorporation into the lattice, a reproducible route toward p-type ZnO is still missing. However, recent experiments could show that p-type conductivity can be generated in the oxide electronic system, although the explanation of the effect is still under debate. Last, but not least, the thermodynamic stability of the ZnO lattice and its propensity to develop well-shaped nanostructures, such as rods, wires, pillars, or coils, make this material so fascinating for applications.^{6,7}

Despite intense research over the last decades, the variety of intrinsic and tailor-made ZnO properties is not under full experimental control, which limits an integration of the oxide into existing technologies. In particular, the role of lattice imperfections, both native defects and impurity ions, is not clear. The main reasons for this ambiguity are (i) the complex interplay between different defects that tend to compensate each other, (ii) difficulties to prepare samples with sufficient purity and structural quality, and (iii) the small number of spatially resolved experiments that are able to identify the

nature of lattice imperfections.⁸ So far, most atomic-scale experiments have been performed with scanning tunneling (STM) and atomic force microscopy (AFM) on single crystals.^{9–12} Such bulk samples often contain an unknown concentration of dopants and defects and only allow for limited spatial resolution due to their low conductivity. Moreover, controlled tailoring of the materials properties, for example, by introducing foreign species, is prohibited when starting with a bulk system.

A promising approach to overcome these drawbacks is the growth of ZnO films on suitable crystalline supports, a technique that provides new degrees of freedom to alter structure and morphology at the atomic scale.^{13,14} ZnO films have been grown on various metal surfaces, such as Ag(111),¹⁵ Pd(111),¹⁶ and recently Pt(111).¹⁷ In all examples, the film quality was found to result from two parameters that are the lattice mismatch with the support and the ability of the films to compensate the intrinsic polarity of the wurzite lattice. The energetically preferred growth direction of ZnO is the (0001) axis, along which Zn and O planes alternate in a regular fashion. To avoid divergence of the electrostatic energy, the associated surface dipole needs to be quenched at a critical film thickness, by either hydroxylation,¹⁸ metallization,^{19,20} or nonstoichiometric surface compositions.^{9,21} Whereas hydroxylation and nonstoichiometric surface oxides^{9,11} are the classical polarity compensation schemes for bulk ZnO, graphitic structures with Zn and O atoms lying in the same plane have been observed for thin films.^{15,16} The graphitic ZnO is stable only in the limit of a few atomic layers ($n < 4$) and evolves to a disordered wurzite

Received: February 25, 2013

Revised: April 24, 2013

Published: April 24, 2013

lattice with increasing thickness. Because of this structural transition, supported ZnO films are often of low structural quality and unsuitable for atomic scale experiments.

In this work, we present a new approach to grow crystalline ZnO films that maintain a high surface quality even at large thicknesses. As a starting point, we have chosen the Au(111) surface that shares the hexagonal symmetry with ZnO(0001) and can be treated at sufficiently high temperature to reach thermodynamic equilibrium. Our preparation allows us to grow ZnO(0001) films of 1–30 ML in thickness, thick enough to develop the band gap of bulk ZnO. On the basis of our experimental results, we discuss the issue of polarity compensation at the oxide surface.

2. EXPERIMENTS

The experiments have been performed in a liquid-nitrogen-cooled STM operated at UHV conditions (2×10^{-10} mbar). The STM head is placed inside a parabolic mirror with the tip being in the focal point.²² A second mirror outside the vacuum chamber directs the light into the entrance slit of a grating spectrograph, being attached to a charge-coupled-device detector. This arrangement allows us to probe small photon fluxes emitted from the STM junction in a broad wavelength range from 200 to 1200 nm. Besides the STM setup, our vacuum chamber is equipped with standard tools for sample preparation and analysis, such as a sputtering gun, a LEED/Auger system, and several e-beam evaporators. The Au(111) single crystal used as the support for the ZnO was cleaned by repeated cycles of Ar⁺ sputtering and annealing to 1100 K. ZnO pellets were evaporated from a Mo crucible in 5×10^{-5} mbar O₂ and deposited onto the clean gold surface at room temperature. The preparation was finalized by annealing the films to temperatures between 600 and 800 K in an O₂ ambient of 5×10^{-5} mbar.

3. RESULTS AND DISCUSSION

3.1. Thickness-Dependent Evolution of the ZnO Morphology.

In the limit of small exposure and high annealing temperature ($T > 750$ K), development of isolated ZnO nanocrystallites is observed on the Au(111) surface (Figure 1a). The typical deposits are up to 6 nm in height and 20 nm in diameter and feature distinct triangular or hexagonal shapes. Their height-to-diameter ratio is around 0.3, indicating that the oxide film already dewets from the metal support at this temperature. As our study aims at closed films, we did not explore the ZnO crystallites any further. Films that cover the entire Au(111) surface have been obtained at higher ZnO load and lower annealing temperature. An example for a film of 1–2 ML in nominal thickness is shown in Figure 1b. Its surface is covered with a hexagonal dot pattern with 2.2 nm periodicity, being assigned to a Moiré superstructure. On the basis of the experimental cell size and the ZnO bulk lattice constant, it is traced back to (7 × 7) ZnO(0001) unit cells overgrowing (8 × 8) cells of the unreconstructed Au(111) support, yielding an hexagonal superstructure with 2.3 nm periodicity (Figure 3). The agreement with the experiment becomes even better when a small lattice expansion (+3%) is assumed for the interfacial ZnO planes. Such a moderate increase seems reasonable, as the wurzite lattice tends to undergo a tetragonal distortion in which the vertical lattice parameter is reduced with respect to the in-plane one in order to lower the film polarity.¹⁵ We note that STM images showing the Moiré superstructure give no hint for

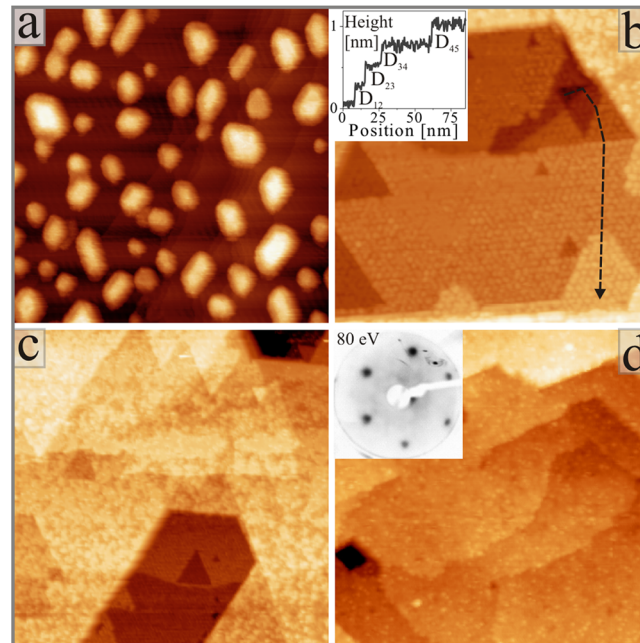


Figure 1. Overview STM images of (a) ZnO nanoislands (1.6 V, 160×160 nm²) and compact films of (b) 3 ML (80×80 nm²), (c) 8 ML (160×160 nm²), and (d) 15 ML (160×160 nm²) in nominal thickness grown on Au(111). The inset in (b) displays a height profile across the first four ZnO layers. Measured step heights are $D_{12} = 2.2$ Å, $D_{23} = 2.4$ Å, $D_{34} = 2.6$ Å, and $D_{45} = 2.6$ Å. The inset (d) shows the LEED pattern of the 15 ML film.

a preservation of the Au(111) herringbone reconstruction beneath the ZnO. We, therefore, suggest that the gold reconstruction is lifted during oxide growth, a behavior that has been found for many other dielectric and molecular overlayers on the Au(111) surface before.²³ Our tentative model, growth of a strained ZnO(0001) layer on the unreconstructed Au(111) surface, gets corroborated by LEED measurements that show only the plain hexagonal spot pattern of ZnO(0001) (Figure 1d, inset). The Moiré structure is not resolved in the diffraction pattern due to the small coherence length of our LEED system and the finite size of continuous superstructure domains.

On the first four oxide layers, the Moiré pattern remains visible in the STM with a constant in-plane periodicity and a constant corrugation (Figure 1c). The measured corrugation of ~1 Å is independent of the bias voltage, suggesting that the contrast is mainly of geometric origin and not induced by a modulated ZnO state density. A more careful analysis reveals that not all Moiré units appear with the same height and the actual corrugation varies between 0.8 and 1.2 Å (Figure 2a). Occasionally, complete cells are missing or groups of neighboring maxima merge into one continuous bright region. The most surprising observation is that, in the fourth layer, the Moiré superstructure suddenly crosses over into a homogeneous surface without apparent periodicity (Figure 2b). This contrast change often occurs in the middle of wide terraces and is not correlated to surface step edges. Our finding suggests that the Moiré contrast does not exclusively arise from changes in the Zn/O binding positions on the Au(111), but gets enhanced by ad-species on the oxide surface. In the thin-film limit, these adsorbates occupy only distinct regions of the Moiré cell, amplifying the superstructure contrast. Beyond the fourth layer, the adsorbates spread onto the surface and the superstructure

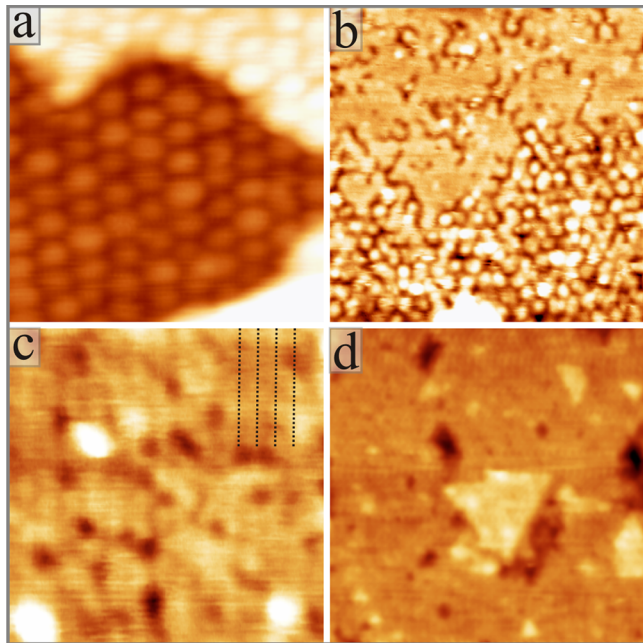


Figure 2. Close-up images of (a) the ZnO/Au(111) Moiré pattern (1st ML, $20 \times 20 \text{ nm}^2$), (b) the transition range between Moiré pattern and flat surface (4th ML, $60 \times 60 \text{ nm}^2$), (c) the (2×1) stripe pattern indicative for a hydrogen superstructure (7th ML, $10 \times 10 \text{ nm}^2$), and (d) the featureless surface of a 15 ML thick film ($100 \times 100 \text{ nm}^2$).

pattern disappears. Note that a Moiré contrast declining with film thickness would be expected if only the modulated Zn/O binding sites at the interface would govern the STM corrugation, in conflict with the experiment. We will show later that the adsorbates on the ZnO(0001) surface are involved in the polarity cancellation.

With increasing film thickness, the Moiré pattern disappears from the topographic images, although the surface retains a mean roughness of $\sim 1 \text{ \AA}$ (Figures 1d, 2d). We believe that the very same ad-species that amplify the Moiré contrast on thin films give rise to the finite corrugation on thicker ones, only that they abandon their long-range order. The ZnO films, on the other hand, remain perfectly crystalline, as proven by the wide, triangular and hexagonal terraces seen in STM. The latter are delimited by straight step edges that follow the equivalent [110] orientations of the Au support. The predominant angle between adjacent steps amounts to 60° , while 120° angles only occur in the case of multiple steps.

3.2. Structure and Morphology of ZnO Films:

Discussion. On the basis of our experimental results and the wealth of literature data on bulk ZnO, we propose the following structure model for the ZnO/Au(111) system. Two factors govern the oxide growth, the polarity of the (0001) wurtzite termination and the lattice mismatch with the Au(111). Interfacial lattice strain seems to be avoided in our case, as the oxide adopts its own lattice parameter right from the beginning. The stacking of two differently sized hexagonal lattices gives rise to the observed Moiré pattern, the dimension of which is best accounted for with a ZnO lattice expanded by +3% grown on top of nonreconstructed Au(111).^{15,16} Note that systems with a stronger interface coupling, such as MgO/Mo(001),²⁴ often develop misfit-driven dislocation networks in order to compensate for the lattice strain.

For the issue of polarity compensation, two balancing effects have to be considered.²⁵ First, the oppositely charged ion planes (Zn^{2+} versus O^{2-}) tend to reduce their mutual distance in order to minimize the associated dipole moment.²⁶ This may converge to graphitic structures, as found for ZnO on Ag(111),¹⁵ where the Zn and O ions reside in the same plane. Second, electron transfer between the oxide overlayer and the metal beneath generates an interface dipole that aligns opposite to the structural ZnO dipole and causes the Zn–O layer distance to increase again.²⁴ At the ZnO/Au interface, charges preferentially flow from the oxide into the electronegative gold, resulting in a stabilization of positively charged Zn^{2+} ions at the interface, while the O^{2-} ions are pushed outward.²⁷ The sum of both effects leads to a situation in which the Zn^{2+} – O^{2-} layer distance is reduced, but not zero as on Ag(111), and the terminating plane is made of oxygen. Indirect evidence for this scenario comes from the reduced step heights measured for the first ZnO layers (2.2 \AA) with respect to thicker films (2.6 \AA , Figure 1b). The Zn^{2+} – O^{2-} layer distance will be additionally modulated by changes in the metal–oxide stacking across the Moiré cell (Figure 3). We expect the largest

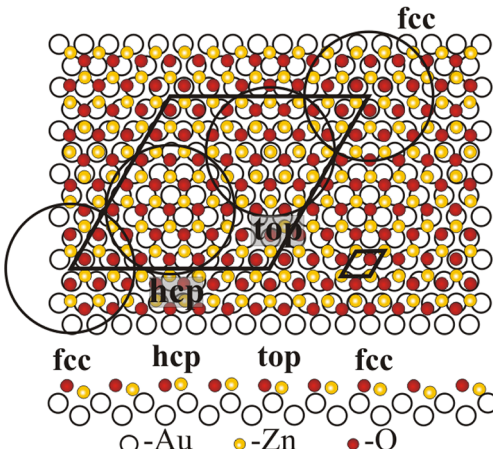


Figure 3. Structure model of the ZnO/Au(111) Moiré cell, showing the three main binding configurations for Zn. Note the modulated Zn–O layer distance in the side view, as discussed in the text.

Zn–O interlayer distance to occur in regions where both, Zn and O ions, occupy Au(111) hollow sites, because the interface distance is small and the charge transfer into the gold is correspondingly big. Conversely, a nearly coplanar and dipole free situation may be adopted by ZnO units in the top domains of the Moiré cell, mimicking the situation of Ag(111) supports where charge-transfer effects are negligible (Figure 3).¹⁵

With increasing film thickness, the ZnO gradually develops a wurtzite structure and a surface dipole builds up. For O-terminated films, being the expected stacking on electronegative gold, this dipole may be canceled with positive excess charges, for example, $\text{Zn}^{\delta+}$ or $\text{H}^{\delta+}$ ions, the density of which is given by the general compensation rule for polar materials: $\sigma_{\text{Surf}} = \sigma_{\text{bulk}}(d/D)$.²⁸ With d the bulk Zn–O layer distance (0.63 \AA) and D the height of the unit cell (2.6 \AA), a surface charge density of $\sigma_{\text{Surf}} = +0.5e/\text{Å}^2$ is required per unit cell. The thickness-dependent dipole becomes critical first in the hollow domains of the Moiré cell, where a finite Zn–O layer distance is present already at the interface and the electrostatic dipole builds up most quickly. In those regions, compensating adsorbates are first attached to the surface and produce the decoration effect

seen in the STM (Figure 2a). Above 4 ML thickness, dipole compensation is required throughout the surface and the decoration effect, hence the Moiré pattern, vanishes from the measurements (Figure 2b). On thick O-terminated ZnO films, dipole compensation may be achieved by either 1/4 ML of Zn^{2+} or 1/2 ML of H^+ ions. We expect our films to be hydrogenated with the simple argument that any excess Zn would immediately oxidize at the O-rich conditions used for preparation. In addition, sufficient amounts of hydrogen are present in the rest gas of our chamber, facilitating surface hydrogenation.²⁹ Hydrogen is known to form a (2 × 1) superstructure on ZnO(0001).^{11,30} Indeed, we are able to identify a faint row pattern on thick ZnO films, which is, however, not perfect but contains numerous defects, for example, H vacancies or H_2O molecules (Figure 2c).

Additional scenarios for the dipole compensation on ZnO(0001) are proposed in the literature. For Zn-terminated ZnO, formation of a nonstoichiometric and oxygen-rich surface oxide was observed that contains a high density of nanometer-sized ad-islands and pits bordered by O-terminated step edges.¹⁰ No equivalent surface reconstruction is revealed in our experiment, and the ZnO terraces are flat down to the atomic scale. In contrast, the large propensity of O-terminated ZnO to develop a compensating hydrogen layer is well-documented in the literature.^{6,31,32} As dipole-compensation depends on the ZnO termination, which, in the case of thin films, is governed by the nature of the metal support, we expect different routes to be active for ZnO on weakly and strongly electronegative substrates, for example, on Ag(111) and Au(111).

3.3. Electronic and Optical Properties of ZnO Films.

The electronic structure of the oxide film and, in particular, the position of the band edges with respect to the Au Fermi level have been probed with STM conductance spectroscopy performed with a lock-in technique and disabled feed back loop. A respective spectrum for a 15 ML thick ZnO film is displayed in Figure 4a. The band onsets show up as steep rises

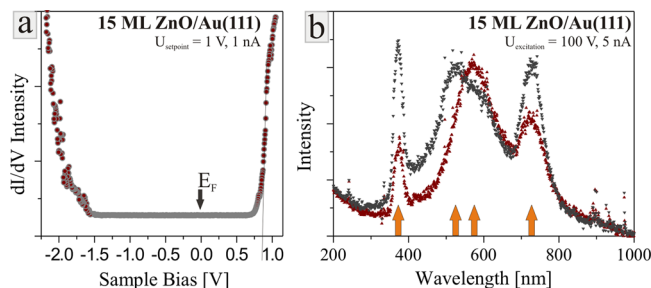


Figure 4. (a) STM conductance spectrum taken on a 15 ML thick ZnO film with a 1.5 V set point bias. Note the upshift of the Fermi level with respect to the band edges, which is typical for an n-type conductor. (b) STM luminescence measured on two similarly prepared ZnO films of 15 ML in thickness. Arrows indicate the four main peaks. While the first peak arises from the electron–hole recombination across the band gap, the following ones are due to defects in the wurzite lattice.

in the dI/dV signal, at -2.0 and $+0.8$ V for valence and conduction band, respectively. The measured band gap of 2.8 eV is, therefore, smaller than the bulk value of 3.4 eV. ZnO on Au(111) exhibits a strong n-type conductance behavior; that is, the Fermi level is much closer to the conduction than to the valence band of the oxide. This finding follows the behavior of

bulk ZnO, which is known to be a strong n-type conductor. The origin of the high ZnO Fermi level is still debated; however, recent DFT calculations³³ and EELS measurements⁴ indicated that H ions in the ZnO lattice are responsible for the partial filling of the conduction band. In our case, the ZnO/Au(111) interface interaction contributes to the n-type conductance characteristic. As discussed before, ZnO loses electrons to the electronegative gold, generating a positive interface dipole that causes the vacuum energy and hence the oxide bands to shift downward. The role of interfacial charge transfer on the band positions of thin oxide films is discussed in detail in the literature, for example, for CaO/Mo(001) films.³⁴ We note that no gap states are detected in the conductance curves, indicating that our ZnO films are reasonably stoichiometric and contain only small amounts of O and Zn defects.

Luminescence spectra of 15 ML thick ZnO/Au(111) films suggest a slightly different picture (Figure 4b). The spectra were obtained via injection of 100 eV electrons (5 nA current) from the STM tip into a predefined sample region of ~ 100 nm in diameter. To minimize electron damage, the acquisition time has been restricted to 120 s and the exposed surface region was changed after each spectral run. More moderate excitation conditions did not yield measurable photon fluxes from ZnO, although already 5 eV electrons were sufficient to generate intense plasmon-mediated light from bare Au(111).³⁵ This finding demonstrates that not an inadequate optical read-out, but an intrinsically low emission yield, renders the high-bias excitation of ZnO/Au films necessary. A typical ZnO emission spectrum (Figure 4b) is characterized by four emission lines, centered at 373 nm (3.3 eV), 535 nm (2.3 eV), 595 nm (2.1 eV), and 730 nm (1.7 eV). Whereas the high- and low-wavelength lines are sharp and distinct (fwhm: $90/180$ meV, respectively), the two central lines are relatively broad (fwhm: 250 meV). The peak at 373 nm is readily assigned to the band-gap recombination of ZnO. Upon high-energy electron impact, hot electrons are excited into the conduction band, from where they relax to the band minimum at the Γ point and recombine radiatively with holes in the valence band.³⁶ We are unable to resolve the excitonic fine structure of the band recombination, partly because of our low spectral resolution, and partly because of the experimental temperature that still enables exciton–phonon coupling.

The other three emission peaks are not intrinsic to stoichiometric ZnO, but point to the presence of defects in the oxide lattice. Whereas donor-type impurities, such as neutral O vacancies and Zn interstitials, induce filled gap states and allow for radiative recombination processes with holes in the valence band, acceptor-type defects, for example, positively charged O defects, give rise to empty gap states and open up new recombination channels for hot electrons in the conduction band.³⁷ Comparing our results with literature data, we remark that the intermediate peaks at 535 and 595 nm are commonly observed in ZnO crystals and nanomaterials.^{38–40} While the peak at 535 nm is assigned to Zn vacancies,^{41,42} the peak at 595 nm is of unknown origin. The 730 nm emission, on the other hand, was found to emerge only after reducing the ZnO by vacuum annealing or electron bombardment, indicating an emission channel mediated by O vacancies.^{36,43} All peaks appear only in thick films, and we, consequently, discard a possible involvement of the ZnO/Au interface in the emission process. We will discuss the nature of

the different emission bands and their dependence on the ZnO preparation conditions in a forthcoming paper.

4. CONCLUSION

Atomically flat and crystalline ZnO films have been prepared on a Au(111) surface and analyzed by means of scanning tunneling microscopy and spectroscopy. The films adopt their own lattice parameter right from the beginning and develop the bulk wurzite structure already at a few-layer thickness. Also, the known electronic and optical properties of the bulk material get quickly established in our films. The intrinsic polarity of the oxide is healed via an adsorbate-mediated mechanism, most likely via hydrogenation. Our preparation method is a good starting point to tailor the properties of ZnO via doping and defect engineering. On this basis, functional oxide films with desired electronic, chemical, and optical properties may be produced in the future.

AUTHOR INFORMATION

Corresponding Author

*E-mail: nilius@fhi-berlin.mpg.de.

Notes

The authors declare no competing financial interest.

ACKNOWLEDGMENTS

F.S. thanks the “Alexander v. Humboldt Stiftung” for a fellowship. The authors acknowledge financial support from the DFG through the Cluster of Excellence “UniCat”.

REFERENCES

- (1) Ozgur, U.; Alivov, Y. I.; Liu, C.; Teke, A.; Reshchikov, M. A.; Dogan, S.; Avrutin, V.; Cho, S. J.; Morkoc, H. A Comprehensive Review of ZnO Materials and Devices. *J. Appl. Phys.* **2005**, *98*, 041301.
- (2) Shan, F. K.; Kim, B. I.; Liu, G. X.; Liu, Z. F.; Sohn, J. Y.; Lee, W. J.; Shin, B. C.; Yu, Y. S. Blueshift of near Band Edge Emission in Mg Doped ZnO Thin Films and Aging. *J. Appl. Phys.* **2004**, *95*, 4772–4776.
- (3) Heo, Y. W.; Kwon, Y. W.; Li, Y.; Pearton, S. J.; Norton, D. P. p-Type Behavior in Phosphorus-Doped (Zn,Mg)O Device Structures. *App. Phys. Lett.* **2004**, *84*, 3474–3476.
- (4) Qiu, H.; Meyer, B.; Wang, Y.; Wöll, C. Ionization Energies of Shallow Donor States in ZnO Created by Reversible Formation and Depletion of H Interstitials. *Phys. Rev. Lett.* **2008**, *101*, 236401.
- (5) Lee, E. C.; Kim, Y. S.; Jin, Y. G.; Chang, K. J. Compensation Mechanism for N Acceptors in ZnO. *Phys. Rev. B* **2001**, *64*, 085120.
- (6) Wang, Z. L. Zinc Oxide Nanostructures: Growth, Properties and Applications. *J. Phys.: Condens. Matter* **2004**, *16*, R829–R858.
- (7) Yi, G.-C.; Wang, C.; Park, W. ZnO Nanorods: Synthesis, Characterization and Applications. *Semicond. Sci. Technol.* **2005**, *20*, S22–S34.
- (8) Likovich, E. M.; Jaramillo, R.; Russell, K. J.; Ramanathan, S.; Narayananmurti, V. Narrow Band Defect Luminescence from Al-Doped ZnO Probed by Scanning Tunneling Cathodoluminescence. *Appl. Phys. Lett.* **2011**, *99*, 151910–151912.
- (9) Parker, T. M.; Condon, N. G.; Lindsay, R.; Leibsle, F. M.; Thornton, G. Imaging the Polar (0001̄) Source and Non-polar (101̄0) Source Surfaces of ZnO with STM. *Surf. Sci.* **1998**, *415*, L1046–L1050.
- (10) Dulub, O.; Diebold, U.; Kresse, G. Novel Stabilization Mechanism on Polar Surfaces: ZnO(0001)-Zn. *Phys. Rev. Lett.* **2003**, *90*, 016102.
- (11) Ostendorf, F.; Torbrügge, S.; Reichling, M. Atomic Scale Evidence for Faceting Stabilization of a Polar Oxide Surface. *Phys. Rev. B* **2008**, *77*, 041405.
- (12) Zheng, H.; Kröger, J.; Berndt, R. Spectroscopy of Single Donors at ZnO(0001) Surfaces. *Phys. Rev. Lett.* **2012**, *108*, 076801.
- (13) Freund, H.-J.; Pacchioni, G. Oxide Ultra-Thin Films on Metals: New Materials for the Design of Supported Metal Catalysts. *Chem. Soc. Rev.* **2008**, *37*, 2224–2242.
- (14) Nilius, N. Properties of Oxide Thin Films and Their Adsorption Behavior Studied by Scanning Tunneling Microscopy and Conductance Spectroscopy. *Surf. Sci. Rep.* **2009**, *64*, 595–659.
- (15) Tusche, C.; Meyerheim, H. L.; Kirschner, J. Observation of Depolarized ZnO(0001) Monolayers: Formation of Unreconstructed Planar Sheets. *Phys. Rev. Lett.* **2007**, *99*, 026102.
- (16) Weirum, G.; Barcaro, G.; Fortunelli, A.; Weber, F.; Schennach, R.; Surnev, S.; Netzer, F. P. Growth and Surface Structure of Zinc Oxide Layers on a Pd(111) Surface. *J. Phys. Chem. C* **2010**, *114*, 15432–15446.
- (17) Martynova, Y.; Liu, B.-H.; McBriarty, M. E.; Groot, I. M. N.; Bedzyk, M. J.; Shaikhutdinov, S.; Freund, H.-J. CO Oxidation over ZnO Films on Pt(1 1 1) at Near-Atmospheric Pressures. *J. Catal.* **2013**, *301*, 227–232.
- (18) Wang, Y. High Resolution Electron Energy Loss Spectroscopy on Perfect and Defective Oxide Surfaces. *Z. Phys. Chem.* **2008**, *222*, 927–966.
- (19) Meyer, B.; Marx, D. Density-Functional Study of Cu Atoms, Monolayers, Films, and Coadsorbates on Polar ZnO Surfaces. *Phys. Rev. B* **2004**, *69*, 235420.
- (20) Wang, Y.; Meyer, B.; Yin, X.; Kunat, M.; Langenberg, D.; Traeger, F.; Birkner, A.; Wöll, Ch. Hydrogen Induced Metallicity on the ZnO(101̄0) Surface. *Phys. Rev. Lett.* **2005**, *95*, 266104.
- (21) King, S. T.; Parihar, S. S.; Pradhan, K.; Johnson-Steigelman, H. T.; Lyman, P. F. Observation of a ($\sqrt{3} \times \sqrt{3}$)R30° Reconstruction on O-Polar ZnO Surfaces. *Surf. Sci. Lett.* **2008**, *602*, L131–L134.
- (22) Freund, H.-J.; Nilius, N.; Risse, T.; Schauermann, S.; Schmidt, T. Innovative Measurement Techniques in Surface Science. *ChemPhysChem* **2011**, *12*, 79–87.
- (23) Yang, G. H.; Liu, G. Y. New Insights for Self-Assembled Monolayers of Organothiols on Au(111) Revealed by Scanning Tunneling Microscopy. *J. Phys. Chem. B* **2003**, *107*, 8746–8759.
- (24) Benedetti, S.; Torelli, P.; Valeri, S.; Benia, H. M.; Nilius, N.; Renaud, G. Structure and Morphology of Thin MgO Films on Mo(001). *Phys. Rev. B* **2008**, *78*, 195411.
- (25) (a) Goniakowski, J.; Giordano, L.; Noguera, C. Polarity of Ultrathin MgO(111) Films Deposited on a Metal Substrate. *Phys. Rev. B* **2010**, *81*, 205404. (b) Davis, T. J.; Vernon, K. C.; Gomez, D. E. Designing Plasmonic Systems Using Optical Coupling between Nanoparticles. *Phys. Rev. B* **2009**, *79*, 155433.
- (26) Goniakowski, J.; Noguera, C.; Giordano, L. Prediction of Uncompensated Polarity in Ultrathin Films. *Phys. Rev. Lett.* **2007**, *98*, 205701.
- (27) Pan, Y.; Benedetti, S.; Valeri, S.; Noguera, C.; Giordano, L.; Goniakowski, J.; Nilius, N. Compensating Edge Polarity: A Means To Alter the Growth Orientation of MgO Nanostructures on Au(111). *J. Phys. Chem. C* **2012**, *116*, 11126–11132.
- (28) Goniakowski, J.; Finocchi, F.; Noguera, C. Polarity of Oxide Surfaces and Nanostructures. *Rep. Prog. Phys.* **2008**, *71*, 016501–016556.
- (29) Meyer, B.; Marx, D.; Dulub, O.; Diebold, U.; Kunat, M.; Langenberg, D.; Wöll, Ch. Partial Dissociation of Water Leads to Stable Superstructures on the Surface of Zinc Oxide. *Angew. Chem., Int. Ed.* **2004**, *43*, 6641–6645.
- (30) Lauritsen, J. V.; et al. Stabilization Principles for Polar Surfaces of ZnO. *ACS Nano* **2011**, *5*, 5987–5994.
- (31) Dulub, O.; Meyer, B.; Diebold, U. Observation of the Dynamical Change in a Water Monolayer Adsorbed on a ZnO Surface. *Phys. Rev. Lett.* **2005**, *95*, 136101.
- (32) Dulub, O.; Boatner, L. A.; Diebold, U. STM Study of the Geometric and Electronic Structure of ZnO(0001)-Zn, (0001̄)-O, (101̄0), and (112̄0) Surfaces. *Surf. Sci.* **2002**, *519*, 201–217.
- (33) Du, M.-H.; Biswas, K. Anionic and Hidden Hydrogen in ZnO. *Phys. Rev. Lett.* **2011**, *106*, 115502.

- (34) Shao, X.; Nilius, N.; Freund, H.-J. Li/Mo Codoping of CaO Films: A Means to Tailor the Equilibrium Shape of Au Deposits. *J. Am. Chem. Soc.* **2012**, *134*, 2532–2534.
- (35) Gimzewski, B. Inelastic Tunneling Excitation of Tip-Induced Plasmon Modes on Noble-Metal Surfaces. *Phys. Rev. Lett.* **1991**, *67*, 3796–3799.
- (36) Zhangl, B. P.; Binhl, N. T.; Segawa1, Y.; Kashiwaba, Y.; Haga, K. Photoluminescence Study of ZnO Nanorods Epitaxially Grown on Sapphire (11̄20) Substrates. *Appl. Phys. Lett.* **2004**, *84*, 586–588.
- (37) Janotti, A.; Van de Walle, C. G. Native Point Defects in ZnO. *Phys. Rev. B* **2007**, *76*, 165202.
- (38) (a) Vanheusden, K.; Warren, W. L.; Seager, C. H.; Tallant, D. R.; Voigt, J. A.; Gnade, B. E. Mechanisms Behind Green Photoluminescence in ZnO Phosphor Powders. *J. Appl. Phys.* **1996**, *79*, 7983–7990. (b) Li, Y.; Cheng, G. S.; Zhang, L. D. Fabrication of Highly Ordered ZnO Nanowire Arrays in Anodic Alumina Membranes. *J. Mater. Res.* **2000**, *15*, 2305–2308.
- (39) Lin, X.; He, X. B.; Yang, T. Z.; Guo, W.; Shi, D. X.; Gao, H.-J.; Ma, D. D. D.; Lee, S. T.; Liu, F.; Xie, X. C. Intrinsic Current-Voltage Properties of Nanowires with Four-Probe Scanning Tunneling Microscopy: A Conductance Transition of ZnO Nanowire. *Appl. Phys. Lett.* **2006**, *89*, 043103–043105.
- (40) Gorla, C. R.; Emanetoglu, N. W.; Liang, S.; Mayo, W. E.; Lu, Y.; Wraback, M.; Shen, H. Structural, Optical, And Surface Acoustic Wave Properties of Epitaxial ZnO Films Grown on (01̄12) Sapphire by Metalorganic Chemical Vapor Deposition. *J. Appl. Phys.* **1999**, *85*, 2595–2603.
- (41) (a) Takata, S.; Minami, T.; Nanto, H. DC EL in Annealed Thin Film of Sputtered ZnO. *Jpn. J. Appl. Phys.* **1981**, *20*, 1759–1762. (b) Tanaka, S.; Takahashi, K.; Sekiguchi, T.; Sumino, K.; Tanaka, J. Cathodoluminescence from Fractured Surfaces of ZnO Varistors. *J. Appl. Phys.* **1995**, *77*, 4021–4024.
- (42) Ton-That, C.; Weston, L.; Phillips, M. R. Characteristics of Point Defects in the Green Luminescence from Zn- and O-Rich ZnO. *Phys. Rev. B* **2012**, *86*, 115205.
- (43) Knutson, K. E.; Galeckas, A.; Zubia, A.; Tuomisto, F.; Farlow, G. C.; Svensson, B. G.; Kuznetsov, A. Yu. Zinc Vacancy and Oxygen Interstitial in ZnO Revealed by Sequential Annealing and Electron Irradiation. *Phys. Rev. B* **2012**, *86*, 121203.